A scoring screening system based on machine learning for immunotherapy beneficiaries in triple-negative breast cancer

Qiheng Gou (douglasgou@foxmail.com)
Sichuan University

Zijian Liu
Sichuan University

Yuxin Xie
Sichuan University

Yulan Deng
Sichuan University

Ji Ma
Sichuan University

Jiangping Li
Sichuan University

Hong Zheng
Sichuan University

Research Article

Keywords: TNBC, TME, PCA, TIDE, Immunotherapy

Posted Date: May 6th, 2022

DOI: https://doi.org/10.21203/rs.3.rs-1605620/v1

Abstract

Background: The role of the tumor microenvironment (TME) in predicting prognosis and therapeutic efficacy has been demonstrated. Nonetheless, no systematic studies have focused on TME patterns or their function in the effectiveness of immunotherapy in triple-negative breast cancer (TNBC).

Methods: In this study, we comprehensively estimated the TME infiltration patterns of 491 TNBC patients from four independent cohorts, and three cohorts that received immunotherapy were used for validation. The TME subtypes were comprehensively evaluated based on immune cell infiltration levels in TNBC, and the TME score was identified and systematically correlated with representative tumor characteristics. Eventually, we sequenced 80 TNBC samples as an external validation cohort to make our conclusions more convincing.

Results: Two distinct TME subtypes were identified and were highly correlated with immune cell infiltration levels and immune-related pathways. More representative TME scores calculated by machine learning could reflect the fundamental characteristics of TME subtypes and predict the efficacy of immunotherapy and prognosis of TNBC patients. A low TME score, characterized by activation of immunity and ferroptosis, indicated an activated TME phenotype and better OS. A high TME score, characterized by the activation of immunosuppressive cells such as CAFs, MDSCs, TAM-M2, cancer stem cells, and a lack of adequate immune infiltration, indicated an immune-suppressed TME phenotype and poorer survival. Low TME scores showed a better response to immunotherapy in TNBC by TIDE analysis and sensitivity to multiple drugs in GDSC analysis. A low TME score showed a significant therapeutic advantage in patients in the three immunotherapy cohorts.

Conclusions: TME subtypes played an essential role in assessing the diversity and complexity of the TME in TNBC. The TME score could be used to evaluate the TME of an individual tumor to enhance our understanding of the TME and guide more effective immunotherapy strategies. Depicting a sweeping landscape of the TME characteristics of TNBC may therefore help to interpret the responses of TNBC to immunotherapies and provide new strategies for the treatment of cancers.

Introduction

Worldwide, breast cancer, accounting for approximately 30% of cancers in women [1], can be divided into three subtypes based on estrogen receptor (ER), progesterone receptor (PR), and HER2 status: hormone receptor-positive; HER2-positive; and triple-negative breast cancer (TNBC) [2]. TNBC, characterized by a lack of ER, PR and HER2 expression, accounts for approximately 15–20% of all breast cancers [3–5]. Higher local recurrence and distant metastasis rates than other breast cancer subtypes are outstanding characteristics of TNBC, resulting in the worst overall survival (OS). Approximately 30% of TNBC patients suffer recurrence within five years of diagnosis [6]; therefore, selecting populations suitable for different treatments of TNBC patients is crucial.

However, previous studies have emphasized the significance of cell–cell interactions and upregulated signaling pathways in regulating the tumor microenvironment (TME) [7,8], suggesting that whole sample intercellular relationships are more vital than transcriptional variations of tumor cells [9,10]. The TME conditions at the baseline level could reflect the immunotherapy efficacy and chemotherapy response rate [11], and various TME cells, such as cytotoxic T cells, tumor-associated macrophages (TAMs), dendritic cells (DCs), and cancer-associated fibroblasts (CAFs), correlated with therapeutic benefits in various tumors, including breast cancer, melanoma and urothelial cancer [12–14]. Understanding the TME instead of cancer cells seems to be a promising method for determining the heterogeneity in breast cancer, and various cells in the TME should be completely described and analyzed [15,16]. Previous studies reported that TNBC was characterized by more abundant immune cell infiltration and higher levels of immune checkpoint inhibitor expression than other breast cancer subtypes [17–19]. Some studies have shown that high levels of lymphocytic infiltration, such as $CD8^+$ T and $CD4^+$ T cells, are consistently correlated with a more favorable prognosis in TNBC [20–22].

Although TNBC patients are challenging to treat and are usually treated with standard chemotherapy and PARP inhibitors [23,24], several clinical trials have reported that immunotherapy might improve the survival of TNBC patients. For instance, the IMpassion130 trial implied that atezolizumab was beneficial in previously untreated metastatic TNBC [25]. The Keynote355 trial reported that pembrolizumab benefited the PDL-1-positive TNBC population in terms of PFS [26]. Although these findings reinforce the perspective that immunotherapy seems more appropriate for TNBC, considerable research is urgent to identify benefit groups from this therapeutic strategy.

A previous study depicted a vast TME landscape of gastric cancer and helped to provide new strategies for interpreting responses to immunotherapies [27]. Considering the lack of rigorous studies on the TME subtype in TNBC, with the emergence of more analytical techniques, two TME-related subtypes were identified by clustering of immune cell infiltration levels. Based on TME-related DEGs and the machine learning method PCA algorithm, a TME scoring system for TNBC patients was constructed and validated in several public datasets. There were several studies based on this dimensionality reduction method, such as a m6A-related score from our previous study [28], a "writer" score model from colorectal cancer [29], and a mast cell-based signature in lung cancer [30]. All these studies constructed a scoring system based on differentially expressed genes among several identified subtypes. Meanwhile, our TME subtypes in TNBC were also highly associated with the activation of related pathways, the cancer stemness index, and drug sensitivity.

Most importantly, the TME score was further employed to predict the immunotherapy responses in TIDE analysis, revealing that we could determine the benefit populations of TNBC patients who received immunotherapy. Interestingly, a twenty-member prognostic signature simplified by the iterative LASSO algorithm could predict the survival probability of TNBC patients and could shrink the TME score calculation members, which had the same ability as the TME score. Eventually, all these analysis results were validated in a TNBC cohort with sequencing data and clinical information.

Methods

Data sources and filtering

The raw data were downloaded from the Gene Expression Omnibus (GEO) (https://www.ncbi.nlm.nih.gov/geo/) and Cancer Genome Atlas (TCGA) databases. Three TNBC datasets (GSE96058 [31], GSE86166 [32], and GSE103091 [33]) and two datasets related to immunotherapy (GSE35640 [34] and GSE78220 [35]) in the GEO database were used for analysis. The pancancer data involving 17 cancer types in TCGA were downloaded from the UCSC XENA database (https://xenabrowser.net/datapages/) [36]. We extracted TNBC data from all TCGA datasets for the principal analysis, and other tumors were used for validation. Moreover, the profiles of the IMvigor210 cohort were obtained according to official guidelines (http://research-pub.Gene.com/imvigor210corebiologies) [13]. All the information of the public datasets is summarized in Table S1.

Tissue Sample Collection and High-throughput Sequencing

In addition, we used a cohort constructed by the West China Hospital breast cancer specialist research team as an external validation cohort, including eighty TNBC biopsies, and this experiment was approved by the Ethics Committee of Western China Hospital. Total RNA was extracted and purified following the manufacturer's protocol. After synthesizing first- and second-strand cDNA using random hexamer primers, DNA Polymerase I and RNase H, the library fragments were purified with an AMPure XP system (Beckman Coulter, Beverly, USA) as described in the NEBNext UltraTM Directional RNA Library following the manufacturer's recommendations. The libraries were then sequenced on the Illumina HiSeq X ten platform (Novogene Bioinformatic Technology Co., Ltd., China) following a 150 bp paired-end read protocol. Eventually, the raw sequencing data from this study have been deposited in the Genome Sequence Archive (GSA) in BIG Data Center (https://bigd.big.ac.cn/) [37], Beijing Institute of Genomics (BIG), Chinese Academy of Sciences, under the accession number HRA002256.

Assessment of immune cell infiltration levels

Single-sample gene set enrichment analysis (ssGSEA) is a well-known method to derive the absolute enrichment scores of previously experimentally validated gene signatures conducted by the R package "GSVA," a nonparametric and unsupervised method commonly employed to estimate the variations in the pathway and biological process activity of a single sample [38]. Here, we preferred to use ssGSEA to assess the relative abundance of immune cell infiltration levels in a single sample. Two validated immune cell signatures published, named immune cell signatures 1 and 2 in this study, were used in this research, containing 24 [39] and 23 [40] types of immune cells, respectively. The markers of these two signatures are listed in Table S2-3. To further validate the results from ssGSEA, the CIBERSORT algorithm [41], which is a deconvolution algorithm, was employed to infer cell-type proportions with bulk tumor sequence data. Moreover, the third method, called Estimation of Stromal and Immune cells in malignant

tumors using Expression data (ESTIMATE) [42,] was also used to infer the fraction of stromal and immune cells in tumor samples.

Functional enrichment analysis

Using ssGSEA described above, GSVA [43] was used to assess pathway activation levels in a single sample with the gene set "c5.all.v6.2. symbols" downloaded from the MSigDB database in GSEA website [44] and another published pathway gene set summarized in Table S4 [13]. GO and Kyoto Encyclopedia of Genes and Genomes (KEGG) analyses were conducted using the R package and the online website Database for Annotation, Visualization, and Integrated Discovery (DAVID) (david.ncifcrf.gov) [45].

Unsupervised clustering and differentially expressed gene analysis.

Unsupervised clustering analysis was used to classify patients based on the immune cell infiltration levels with the ConsensuClusterPlus package [46]. Differentially expressed gene (DEGs) analysis was conducted by the "limma" R package, with criteria of adjusted P value < 0.05. The differentially expressed mRNAs were visualized by the "pheatmap" package.

Calculation of the ferroptosis index (FPI) and mRNA-based stemness index (mRNAsi)

A total of 113 ferroptosis regulators were extracted from the online website FerrDb (http://www.zhounan.org/ferrdb/), and the specific information of these genes is shown in Table S5. To describe the ferroptosis level, FPI was established based on the expression data of genes in ferroptosis, including positive and negative components. The enrichment score (ES) was calculated using ssGSEA, and the FPI to roughly assess ferroptosis trends was calculated as follows:

FPI = ES (positive) – ES (negative) [47]

To assess the stemness of cancer cells, a one-class logistic regression algorithm called mRNAsi was used to calculate the stemness index for each sample under the direction of the workflow available on a previously established database (https://bioinformaticsfmrp.github.io/) [48].

Therapeutic Response Prediction

The chemotherapeutic response for TNBC was predicted according to the data involved in the Genomics of Drug Sensitivity in Cancer (GDSC) with the "pRRophetic" package [49]. The Tumor Immune Dysfunction and Exclusion (TIDE) database (http://tide.dfci.harvard.edu/) was employed to predict the immunotherapy response of TNBC [50], and the default cutoff value was 0.

Calculation of TME Score

The overlapping DEGs among the four TNBC datasets were regarded as TME gene signatures. Principal component analysis (PCA) was used to calculate the TME score to quantize the TME patterns in TNBC.

We summed PC1 and PC2 of genes i by PCA as we described before [28]. The TME score was calculated as follows:

TME score = Σ (PC1i + PC2i)

Prognostic signature construction and survival analysis

Logistic least absolute shrinkage and selection operator (LASSO) regression analysis can construct a prognostic signature to minimize the risk of overfitting [51]. However, LASSO relies heavily on seeds when it allows. Iteration LASSO was independent of seed once the roots were changed, the optimal lambda changed, and the resulting feature changed [52]. The features retained at high frequency can be considered the most influential factors. Genes included under consensus were generated by iteration of LASSO, and AUC further selected the minimum combination of genes associated with survival. The formula of patients' risk scores was established:

Risk score = Σ (each gene's expression × corresponding coefficient).

Receiver operating characteristic (ROC) curves and survival curves with the Kaplan–Meier method were used to judge the prediction efficiency of the signature. The best cutoff value of genes in survival analysis was searched by the "survminer" R package. The signature genes obtained from iterated LASSO analysis were used for nomogram construction using logistic and Cox regression analyses. Calibration curves were used to assess the predictive accuracy of the nomogram.

Statistical Analysis

Correlation coefficients and p values were calculated by Spearman correlation analysis among several defined groups. Wilcoxon tests were used to compare differences between the two groups. The asterisks represent the statistical p values (*P < 0.05; **P < 0.01; ***P < 0.001) in the panels.

Results

Identification of TME Subtypes

To explore the tumor microenvironment patterns in four independent TNBC cohorts, consensus cluster analysis was used to classify patients with TME conditions (Figure S2A-D). By integrating the clustering results of each dataset, two distinct TME subtypes were eventually identified using unsupervised clustering in each cohort, named subtypes 1 and 2 (Figure 1A). Here, we used immune cell signature 1 to perform cluster analysis. At the same time, we found that the infiltration of the levels of immune cells was significantly different using immune cell signature 2 in all four cohorts (Figure 1B). Among them, subtype 1 was enriched with immune cells compared with subtype 2, meaning that subtype 1 was an immune-activating subtype with higher immune cell infiltration levels, the same as the conception of a "hot" tumor. By the CIBERSORT algorithm, we found that some antitumor immune cells, such as CD8+ T cells, activated CD4+ T cells and M1-like macrophages, were higher in subtype 1. In contrast, tumor-

associated immune cells, such as M2-like macrophages, were more elevated in subtype 2 (Figure 1C-D). Given these differences in the TME for these two subtypes, survival analysis showed that the overall survival of subtype 1 in the four cohorts was better than that of subtype 2 (Figure 1E).

Biological Function Analysis between TME subtypes

To further investigate the differences between the two TME subtypes, we considered analyzing the biological function variation in the conception of signaling pathways. GSVA showed that all immune-related pathways, such as the IL-2/STAT5, IL-6/STAT3, and interferon response pathways, were enriched in subtype 1, while the TGF-β-, NOTCH-, PI3K/AKT-, and EMT-related pathways were enriched in subtype 2 (Figure 2A-B). ssGSEA with curated signaling pathway signatures showed that the CD8 T effector- and immune checkpoint-related pathways were activated in subtype 1. In contrast, tumor progression-related pathways such as WNT and EMT were activated in subtype 2 (Figure 2C-D). Traditional GSEA was also conducted between subtypes in the four cohorts, which was consistent with the above results (Figure S3A). Using the ESTIMATE method, scores of stromal and immune cells were also higher in subtype 1 (Figure S3B). The expression levels of MHC molecules and immune checkpoint inhibitors (ICIs) are correlated with the activation of the antitumor immune response and the efficacy of immunotherapy. Most MHC molecules and ICIs were significantly different between the two subtypes and were especially higher in subtype 1 (Figure S3C). For a more comprehensive analysis of the two subtypes, we found that the ferroptosis index (FPI) and mRNA-based stemness index (mRNAsi) were higher in subtype 1 than in subtype 2. However, no significant difference was found in tumor mutation burden (TMB) (Figure S3D-F).

Moreover, based on ATAC-seq data from TCGA, differentially expressed peaks were identified between subtypes 1 and 2 (Figure 3E). GO analysis was processed on these differentially expressed peaks annotated by ChIPseeker, and the results showed that genes correlated with T-cell activation had higher chromatin activities in subtype 1. In comparison, genes correlated with the regulation of GTPase and cell morphogenesis possessed higher chromatin activities in subtype 2 (Figure 3F).

Generation of TME score and functional verification

To further investigate the underlying mechanisms between the two TME subtypes, differentially expressed gene (DEG) analysis was conducted in four TNBC cohorts. Taking the intersection of DEGs in four cohorts (Figure 3A-B), 236 TME-related DEGs were identified between TME subtypes, and all of them were upregulated in subtype 1 (Table S6; Figure 3C). GO analysis showed that DEGs were highly enriched in T-cell activation and cell adhesion pathways (Figure 3D). For further analysis, a continuous variable called the TME score by PCA was generated to quantify the different levels of TME in individual patients. The TME score could well reflect the differences in TME subtypes in TNBC cohorts, and the TME score was lower in subtype 1 (Figure S4A). Patients with low TME scores demonstrated a greater survival benefit than patients with high TME scores (Figure 3E-F). ssGSEA calculated with immune cell signature 1 showed that the infiltration levels of most immune cells were highly negatively associated with the TME

score (Figure 3G), and ssGSEA calculated with immune cell signature 2 also verified that most of the immune cells were higher in the low TME score groups (Figure 3H). CIBERSORT analysis showed that as the TME score was reduced, the percentage of cytotoxic T cells increased (Figure 3I). GSVA showed that immune-related pathways, such as the IL-2/STAT5, IL-6/STAT3, and interferon response pathways, were negatively correlated with the TME score.

In contrast, glycolysis, the NOTCH signaling pathway, and protein secretion were positively correlated with the TME score (Figure S4B). ssGSEA with curated pathway signatures verified that the TME score was negatively linked with antigen processing machinery, CD8 T effector, and immune checkpoint and positively associated with WNT target pathways (Figure S4C). We show the genes involved in the above-curated pathway signatures with statistical significance in Figure S4D. Most of the genes involved in immune-related pathways were highly negatively correlated with the TME score. The stromal and immune scores calculated by ESTIMATE were undoubtedly negatively correlated with TME scores in all TNBC cohorts (Figure S4E). The low TME score group still had a higher FPI than the high TME score group, but the mRNAsi and TMB showed no significant differences (Figure S4F-H). Due to differences in FPI between TME subtypes and TME score groups, correlation analysis was conducted between TME score and the expression of ferroptosis-related genes. We found that the expression of TNFAIP3, SOCS1, IFNG, ATM, ALOX5, PML, ISCU, and GCH1 was significantly negatively correlated with TME scores in four TNBC cohorts (Figure S4I). The TME score showed no significant differences between the AJCC_T, AJCC_N, and stage groups, meaning that the TME score was a novel factor regardless of clinical traits (Figure S4J).

The role of the TME score in therapy efficacy

To explore the association between the TME score and drug response, we evaluated the estimated IC50 value of 138 drugs included in the GDSC database in four TNBC cohorts. Correlation analyses were conducted between the TME score and predicted IC50 values (Figure S5A). Drugs with significant differences in more than three cohorts were regarded as potential therapeutic drugs; we found that 8 drugs were sensitive to the high TME score group, and 49 drugs were sensitive to the low TME score group (Figure 4A). The TME score might logically be related to the efficacy of immunotherapy due to its apparent association with immune cell infiltration and activation. TIDE was utilized to predict the immunotherapy response of TNBC patients, and the TME score was lower in the immunotherapy response group (Figure 4B). Moreover, TIDE analysis showed that the TME score was apparently negatively correlated with markers of immunotherapy response and positively correlated with CAFs, myeloid-derived suppressor cells (MDSCs), and TAM M2 (Figure 4C). Lacking TNBC datasets that received immunotherapy, we selected three cohorts that received anti-PDL1, anti-PD1, and anti-MAGE-A3 therapy in bladder cancer (BLCA) and skin melanoma (SKCM) to verify the immunotherapy response prediction value of the TME score. First, TME scores were calculated across cancers in TCGA. TME scores were prognostic risk factors (Figure S5B) and were negatively correlated with immune cell infiltration levels in most cancer types, especially in BLCA and SKCM (Figure 4D). Then, we calculated the TME score in the three immunotherapy cohorts. Interestingly, we found that the TME score was also a risk factor in IMvigor210 (Figure S5C), and patients with a high TME score and low TMB presented the worst

survival advantage (Figure 4E). Correlation analysis further validated that the TME score was negatively correlated with the expression of MHC, costimulatory, and adhesion molecules (Figure S5D) and immune cell infiltration levels (Figure 4F). Moreover, a higher TME score was associated with disease progression (PD) and desert-resistant phenotypes (Figure 4G-I). In the anti-MAGE-A3 cohort, the TME score was also negatively correlated with immune cell infiltration levels (Figure 4J) and was lower in the response group (Figure 4K). Similar results could be seen in the anti-PD1 cohort (Figure 4L), although the differences among response groups showed no significance (Figure S5E).

Verification of the TME score in the external validation TNBC cohort

The TME score was calculated as described above in 80 triple-negative breast cancer samples from the Western China Hospital (TNBC_WC) cohort. It was found that a higher TME score was related to the disease progression rate (Figure 5A) and poor survival probability (Figure S5F) of TNBC patients. ssGSEA also showed a strong correlation between the TME score and immune cell infiltration levels in TNBC_WC (Figure 5B) as well as the results of the ESTIMATE score (Figure 5C). Some MHC molecules and ICI targets were also negatively correlated with the TME score, especially PDL1 and PDCD1LG2 (Figure 5D). For pathway analysis, pathways that were associated with the TME score in TNBC_WC were almost the same as the results in the four training cohorts (Figure 5E). Correlation analysis showed that the TME score was positively correlated with the FPI and mRNAsi (Figure 5F). The response group predicted by TIDE analysis showed a lower TME score than the no response group (Figure 5G). Additionally, we predicted the drug IC50 by GDSC analysis and performed correlation analysis with the TME score (Figure 5H) and intersection drugs with the results in the training cohorts, as shown in Figure 5I. These results illustrated that the TME score was a novel and robust method to measure immune cell infiltration levels and therapy efficacy.

Prognostic signature construction and simplification of the TME score

Considering the accessibility of the TME score, we aimed to shrink the members of the TME score and simplify the formula modes to predict the prognosis of TNBC patients. First, survival analysis was processed for 236 TME-related DEGs in TCGA cohorts; 84 genes with a P value < 0.05 were selected for further research (Figure S6A). Here, iteration LASSO was then used to simplify the members of the TME score; after multiple attempts to reach the highest 5-year AUC, we finally constructed a prognostic signature with 20 members from TME score members (Table S7; Figure 6A). We could see that there were 20 genes with the most frequencies of occurrence in 1000 operation iterations in LASSO algorithms, and prognostic signatures with these 20 genes could reach a high area under the curve (AUC) of ROC for 5 years of survival in the TCGA cohort. To provide a convenient approach for predicting the survival probability of a patient with TNBC, we constructed predictive nomograms with the 20 genes generated above. We developed a nomogram based on the Cox regression model to predict the 5- and 8-year survival probability for TNBC patients (Figure S6B). The calibration plots for the 5- and 8-year survival showed an optimal agreement between the nomogram-predicted and observed OS, which was used to evaluate the accuracy of the prediction signature (Figure 6B). For validation of the prognostic value of the

20-gene signature, the patients in the high-risk group showed a worse prognosis than those in the low-risk group, and the same condition could be seen in other TNBC cohorts (Figure S6C). Before the prognostic signature was constructed, we conducted a correlation analysis between the TME score and the expression of 236 TME-related DEGs in four TNBC cohorts. In view of most genes highly correlated with the TME score, we supposed to simplify the TME score by these 20 genes. Surprisingly, the simplified TME score (sTME score) calculated based on the expression of these 20 genes was highly positively correlated with the TME score in the TNBC_WC cohort (Figure 6C), and patients in the high sTME score group also showed worse DFS than those in the low sTME score group (Figure 6D). Not unexpectedly, the correlation coefficients between the TME score and sTME score were almost close to 1 in other cohorts, which means they were virtually interchangeable (Figure 6E). However, the risk score showed no significance with the TME score, indicating that the risk score was a novel factor generated by the iterative LASSO regression model. Eventually, we set up a coexpression network for 20 genes, and we found strong correlations among them (Figure 6F). The visualization of attribute changes in individual patients using an alluvial diagram indicated that the TME score might be a powerful method to direct therapeutic efficacy or prognostic risk for TNBC patients (Figure 6G).

Discussion

The evolving immunotherapy of malignant tumors inspired our interest in the role of tumor microenvironment patterns in TNBC. The TME, a critical regulator of disease progression and therapeutic outcome, correlates with patient response to immunotherapy in multiple cancers, with patients possessing immune-favorable TME subtypes benefiting the most from immunotherapy [53–55]. However, previous studies reported that breast cancer was generally considered a low immune-reactive cancer, TNBC, the most aggressive subtype of breast cancer, but responded to anti-PD-1/PD-L1 immunotherapy [56,57]. The urgent question is which types of TNBC patients are suitable for immunotherapy and what their characteristics are. This study was the first to identify TME subtypes of TNBC and TME-related DEGs represented for each subtype based on consensus clustering analysis. For a more rigorous conclusion, at least two cross-validation methods were chosen for each step, ssGSEA, CIBERSORT, and ESTIMATE, for assessing immune cell infiltration levels and GSEA GSVA and GO analysis for evaluating pathway activation conditions.

Moreover, multiple cohorts were selected for training or validation, and one private external validation cohort was specialized to collect for confirmation of results. All these innovations will directly differentiate our study of TME patterns in TNBC from all previous studies; there were no systematic studies on the selection of immunotherapy beneficiaries in TNBC based on TME subtypes. The essential light spot of our studies illustrated that two perfect scoring systems based on one gene signature were constructed to predict the efficacy of immunotherapy, response to chemotherapy, and prognosis of TNBC patients.

Previous studies related to the TME score in TNBC [58–60] generally used one method to assess immune cell infiltration levels and did not consider immune-related pathway activation conditions; our study used

not only numerous methods to evaluate immune cell infiltration levels but also employed different types of pathway signatures to evaluate pathway enrichment levels. These results provide mechanistic insights into the efficacy of immunotherapy, suggesting that benefits from immunotherapy are not only related to enhanced IL-2/STAT5, IL-6/STAT3, and interferon response pathways but are also associated with inhibition of TGF-β-, NOTCH-, PI3K/AKT-, and EMT-related pathways. Subtype 1 was characterized by multiple infiltrating immune cells, especially cytotoxic cells and antigen-presenting cells, which were reported to correspond to the resistant activated phenotype [61–63]. In contrast, subtype 2 was characterized by a lack of immune cell infiltration, corresponding to the immune-suppressed phenotype, which is often referred to as a "cold" tumor [64]. Most importantly, based on a machine learning method, the PCA score, we successfully converted categorical variables of TME subtypes to numeric variables of the TME score, which could inherit all characteristics of TME subtypes. The lower the TME score was, the more likely the patient was to be grouped into subtype 1, indicating better immune cell infiltration levels. The lack of TNBC cohorts that received immunotherapy, TIDE analysis, and immunotherapy cohorts in other tumors were utilized to assess the true power of the TME score in the prediction of immunotherapy efficacy. We already know that many TNBC patients could benefit from immunotherapy from the Impassion130 study [65,66], which was highly consistent with our research. The former critical analysis failed to answer the question of benefit group selection; however, our studies showed that some TNBC patients might have a higher possibility of benefitting from immunotherapy, and the specific cutoff value still needs to be further explored. Although this conclusion failed to be validated in the Impassion130 study due to data permission, we successfully validated the efficacy of the TME score in other immunotherapy cohorts in metastatic urothelium carcinoma and melanoma treated with anti-PDL1, anti-PD1, and anti-MAGE-A3.

Correlation analysis between TIDE results members and TME score showed that TME score was highly positively correlated with CAFs, TAM M2, MDSC, and all these cells were reported to be immune suppressive cells and closely associated with cancer stemness [67–69]. Subsequent mRNAsi analysis verified these findings that the TME score was positively correlated with cancer stemness, which might be why subtype 2 was related to progression and metastasis-related pathways and poor immune cell infiltration levels. Cancer stemness has been reported to be associated with immunotherapy efficacy in many studies [70–72], as well as with drug resistance in TNBC [73,74]. Combined with drug information and sequence data in GDSC, several molecular compounds that might be sensitive in TNBC patients have been identified, broadening the drug research direction of basic experiments in TNBC. Ferroptosis, an iron-dependent form of nonapoptotic cell death that is lethal, has received widespread attention as a potential therapeutic pathway for cancer treatment [75,76]. In our research, the ferroptosis level viewed by FPI was higher in subtype 1, meaning that the ferroptosis level might be correlated with an immune-activated TME, and some drugs that infect the ferroptosis process might be sensitive in these patients.

TNBC is a malignant tumor with poor prognosis, and local recurrence, distant metastasis, and drug-resistant resistance have been the leading cause of death [77,78]. The constructed TME subtypes and TME score in this study could reasonably predict the risk of overall survival and had no correlation with

previously defined clinical grade and stages, meaning that this score might be a novel factor unaffected by clinical traits. To better predict the survival possibility of TNBC patients, an iterative LASSO algorithm was conducted in TCGA cohorts and validated in three GEO cohorts. Nomograms to indicate survival possibility and death odds were both established by Cox and logistic regression models, which might be helpful in clinical practice. Interestingly, 20 predictive models were accidentally found to construct a simplified TME score, which might be the same as the TME score built by 236 DEGs. If the TME score could be used in clinical practice to predict immunotherapy and chemotherapy efficacy or prognosis of TNBC patients, we suggest that a simplified TME score might be a more convenient test model.

For 20 genes involved in the predictive signature, we found that these 20 genes were highly associated with immune cell infiltrations in the TME, such as DCs, B cells and T cells, which were comprehensively reported to be associated with immunotherapy efficacy [79–84]. LAMP3, IDO1, HSD11B1, and CD1B are markers of DCs, HLA-DOB and CR2 are markers of B cells, and SIT1, IFNG, ICOS, and CXCL13 are markers of T cells. Although some genes were not markers of immune cells, they were reported to be associated with the TME and immunotherapy efficacy. The expression of SLAMF8 [85] and PSMB8 [86] could predict the efficacy of immune checkpoint inhibitor immunotherapy in gastrointestinal cancer and melanoma. IKZF3 deficiency could potentiate chimeric antigen receptor T cells to target solid tumors [87,] and activation of the GPR171 pathway could suppress T-cell activation and limit antitumor immunity [88]. Several immune-related molecules, including LGALS2, GFI1, and GBP1/5, have not yet been reported to be related to immunotherapy. Eventually, these results further demonstrated that simplifying the TME score by 20 immune-related genes was a perfect signature highly correlated with immune cell infiltration levels to predict immunotherapy efficacy.

Although the TME score could reasonably predict the efficacy of immunotherapy and prognosis of TNBC patients, to validate all the above analyses in public datasets, we finally collected 80 TNBC patients in West China Hospital and performed high-throughput sequencing. The TME score showed powerful abilities in prognostic prediction and assessing immune cell infiltration levels. Importantly, this cohort was also one of the few sequenced data with clinical information in TNBC; however, patients in this cohort had not yet received immunotherapy. From the TIDE and GDSC analysis results in this cohort, immunotherapy and several drugs identified in the above research were also validated.

Conclusion

In conclusion, the TME score was a convenient method to comprehensively classify the TME subtypes and their corresponding characteristics and pathway activation levels in TNBC. It could also be used to assess some cancer-related features, including the ferroptosis index, genetic variation, drug sensitivity, and mRNAsi of individual patients, and further predict the response to immunotherapy of TNBC patients. Importantly, this study provides a perspective for the comprehensive evaluation of the cellular, molecular, and genetic factors associated with TME infiltration patterns to further reverse TME cell infiltration characterization into "hot tumors", thus improving the response to an immune checkpoint inhibitor.

Abbreviations

TNBC: Triple-negative Breast Cancer; ER: Estrogen Receptor; PR: Progesterone Receptor; DFS: Disease-Free Survival; OS: Overall Survival; CAFs: Cancer-associated Fibroblasts; DCs: Dendritic Cells; TAMs: Tumor-associated Macrophages; TME: Tumor Microenvironment; GEO: Gene Expression Omnibus; TCGA: The Cancer Genome Atlas; ssGSEA: Single-sample Gene Set Enrichment Analysis; GSEA: Gene Set Enrichment Analysis; GSVA: Gene Set Variation Analysis; ESTIMATE: Estimation of Stromal and Immune Cells in Malignant Tumors using Expression Data; GO: Gene Ontology; DAVID: Database for Annotation, Visualization and Integrated Discovery; KEGG: Kyoto Encyclopedia of Genes and Genomes; mRNAsi: mRNA-based Stemness Index; FPI: Ferroptosis Index; DEGs: Differentially Expressed Genes; PCA: Principal Component Analysis; HR: Hazard Ratios; LASSO: Logistic Least Absolute Shrinkage and Selection Operator (LASSO); ROC: Receiver Operating Characteristic; AUC: Area Under the Curve; ICI: Immune Checkpoint Inhibitors; TMB: Tumor Mutation Burden; TIDE: Tumor Immune Dysfunction and Exclusion; sTME:

Declarations

Ethics approval and consent to participate

The patient data in this work were acquired from publicly available datasets whose informed consent was complete. A total of eighty TNBC biopsies were collected from the breast cancer biobank of Western China Hospital. This experiment was approved by the Ethics Committee of Western China Hospital.

Consent for publication

Not applicable

Availability of data and materials

All data used in this work can be acquired from the Gene-Expression Omnibus (GEO; https://www.ncbi.nlm.nih.gov/geo/) and UCSC XENA databases (https://xenabrowser.net/datapages/). The raw sequencing data for 80 TNBC samples in this study have been deposited in the Genome Sequence Archive (GSA) in BIG Data Center (https://bigd.big.ac.cn/) under the accession number HRA002256.

Competing interests

The authors declare that they have no competing interests.

Funding

This work was supported by Youth Program of National Natural Science Foundation of China (81902723).

Authors' contributions

Conceptualization: Qiheng Gou. Data curation: Zijian Liu、Yuxin Xie, Hong Zheng. Project administration: Qiheng Gou. Supervision: Qiheng Gou.Writing-original draft: Qiheng Gou、Zijian Liu. Revision: Qiheng Gou、Zijian Liu、Yulan Deng、Jiangping Li、Ji Ma、Hong Zheng. All authors made a significant contribution to the work reported, gave final approval of the version to be published; have agreed on the journal to which the article has been submitted; and agree to be accountable for all aspects of the work.

Acknowledgments

Not applicable

References

1. Siegel RL, Miller KD, Jemal A. Cancer statistics, 2020. CA Cancer J Clin. 2020;70(1):7-30.
2. Denkert C, Liedtke C, Tutt A, von Minckwitz G. Molecular alterations in triple-negative breast cancer-the road to new treatment strategies. Lancet. 2017;389(10087):2430-42.
3. Michel LL, von Au A, Mavratzas A, Smetanay K, Schutz F, Schneeweiss A. Immune Checkpoint Blockade in Patients with Triple-Negative Breast Cancer. Target Oncol. 2020;15(4):415-28.
4. Marra A, Viale G, Curigliano G. Recent advances in triple negative breast cancer: the immunotherapy era. BMC Med. 2019;17(1):90.
5. Adams S, Gatti-Mays ME, Kalinsky K, Korde LA, Sharon E, Amiri-Kordestani L, et al. Current Landscape of Immunotherapy in Breast Cancer: A Review. JAMA Oncol. 2019;5(8):1205-14.
6. Lin NU, Vanderplas A, Hughes ME, Theriault RL, Edge SB, Wong YN, et al. Clinicopathologic features, patterns of recurrence, and survival among women with triple-negative breast cancer in the National Comprehensive Cancer Network. Cancer. 2012;118(22):5463-72.
7. Quail DF, Joyce JA. Microenvironmental regulation of tumor progression and metastasis. Nat Med. 2013;19(11):1423-37.
8. Su S, Chen J, Yao H, Liu J, Yu S, Lao L, et al. CD10(+)GPR77(+) Cancer-Associated Fibroblasts Promote Cancer Formation and Chemoresistance by Sustaining Cancer Stemness. Cell. 2018;172(4):841-56 e16.
9. Mantovani A, Marchesi F, Malesci A, Laghi L, Allavena P. Tumour-associated macrophages as treatment targets in oncology. Nat Rev Clin Oncol. 2017;14(7):399-416.
10. Kalluri R. The biology and function of fibroblasts in cancer. Nat Rev Cancer. 2016;16(9):582-98.
11. Rosenberg JE, Hoffman-Censits J, Powles T, van der Heijden MS, Balar AV, Necchi A, et al. Atezolizumab in patients with locally advanced and metastatic urothelial carcinoma who have

progressed following treatment with platinum-based chemotherapy: a single-arm, multicentre, phase 2 trial. Lancet. 2016;387(10031):1909-20.

12. Nishino M, Ramaiya NH, Hatabu H, Hodi FS. Monitoring immune-checkpoint blockade: response evaluation and biomarker development. Nat Rev Clin Oncol. 2017;14(11):655-68.
13. Mariathasan S, Turley SJ, Nickles D, Castiglioni A, Yuen K, Wang Y, et al. TGFbeta attenuates tumour response to PD-L1 blockade by contributing to exclusion of T cells. Nature. 2018;554(7693):544-8.
14. Lee K, Hwang H, Nam KT. Immune response and the tumor microenvironment: how they communicate to regulate gastric cancer. Gut Liver. 2014;8(2):131-9.
15. Mejia-Pedroza RA, Espinal-Enriquez J, Hernandez-Lemus E. Pathway-Based Drug Repositioning for Breast Cancer Molecular Subtypes. Front Pharmacol. 2018;9:905.
16. Cagan R, Meyer P. Rethinking cancer: current challenges and opportunities in cancer research. Dis Model Mech. 2017;10(4):349-52.
17. Denkert C, von Minckwitz G, Darb-Esfahani S, Lederer B, Heppner BI, Weber KE, et al. Tumour-infiltrating lymphocytes and prognosis in different subtypes of breast cancer: a pooled analysis of 3771 patients treated with neoadjuvant therapy. Lancet Oncol. 2018;19(1):40-50.
18. Loi S, Drubay D, Adams S, Pruneri G, Francis PA, Lacroix-Triki M, et al. Tumor-Infiltrating Lymphocytes and Prognosis: A Pooled Individual Patient Analysis of Early-Stage Triple-Negative Breast Cancers. J Clin Oncol. 2019;37(7):559-69.
19. Mittendorf EA, Philips AV, Meric-Bernstam F, Qiao N, Wu Y, Harrington S, et al. PD-L1 expression in triple-negative breast cancer. Cancer Immunol Res. 2014;2(4):361-70.
20. Savas P, Salgado R, Denkert C, Sotiriou C, Darcy PK, Smyth MJ, et al. Clinical relevance of host immunity in breast cancer: from TILs to the clinic. Nat Rev Clin Oncol. 2016;13(4):228-41.
21. Jang N, Kwon HJ, Park MH, Kang SH, Bae YK. Prognostic Value of Tumor-Infiltrating Lymphocyte Density Assessed Using a Standardized Method Based on Molecular Subtypes and Adjuvant Chemotherapy in Invasive Breast Cancer. Ann Surg Oncol. 2018;25(4):937-46.
22. Gao G, Wang Z, Qu X, Zhang Z. Prognostic value of tumor-infiltrating lymphocytes in patients with triple-negative breast cancer: a systematic review and meta-analysis. BMC Cancer. 2020;20(1):179.
23. Robson M, Im SA, Senkus E, Xu B, Domchek SM, Masuda N, et al. Olaparib for Metastatic Breast Cancer in Patients with a Germline BRCA Mutation. N Engl J Med. 2017;377(6):523-33.
24. Telli ML, Hellyer J, Audeh W, Jensen KC, Bose S, Timms KM, et al. Homologous recombination deficiency (HRD) status predicts response to standard neoadjuvant chemotherapy in patients with triple-negative or BRCA1/2 mutation-associated breast cancer. Breast Cancer Res Treat. 2018;168(3):625-30.
25. Schmid P, Adams S, Rugo HS, Schneeweiss A, Barrios CH, Iwata H, et al. Atezolizumab and Nab-Paclitaxel in Advanced Triple-Negative Breast Cancer. N Engl J Med. 2018;379(22):2108-21.
26. Cortes J, Cescon DW, Rugo HS, Nowecki Z, Im SA, Yusof MM, et al. Pembrolizumab plus chemotherapy versus placebo plus chemotherapy for previously untreated locally recurrent

inoperable or metastatic triple-negative breast cancer (KEYNOTE-355): a randomised, placebo-controlled, double-blind, phase 3 clinical trial. Lancet. 2020;396(10265):1817-28.

27. Zeng D, Li M, Zhou R, Zhang J, Sun H, Shi M, et al. Tumor Microenvironment Characterization in Gastric Cancer Identifies Prognostic and Immunotherapeutically Relevant Gene Signatures. Cancer Immunol Res. 2019;7(5):737-50.
28. Liu Z, He J, Han J, Yang J, Liao W, Chen N. m6A Regulators Mediated Methylation Modification Patterns and Tumor Microenvironment Infiltration Characterization In Nasopharyngeal Carcinoma. Front Immunol. 2021;12:762243.
29. Chen H, Yao J, Bao R, Dong Y, Zhang T, Du Y, et al. Cross-talk of four types of RNA modification writers defines tumor microenvironment and pharmacogenomic landscape in colorectal cancer. Mol Cancer. 2021;20(1):29.
30. Bao X, Shi R, Zhao T, Wang Y. Mast cell-based molecular subtypes and signature associated with clinical outcome in early-stage lung adenocarcinoma. Mol Oncol. 2020;14(5):917-32.
31. Brueffer C, Vallon-Christersson J, Grabau D, Ehinger A, Hakkinen J, Hegardt C, et al. Clinical Value of RNA Sequencing-Based Classifiers for Prediction of the Five Conventional Breast Cancer Biomarkers: A Report From the Population-Based Multicenter Sweden Cancerome Analysis Network-Breast Initiative. JCO Precis Oncol. 2018;2.
32. Prabhakaran S, Rizk VT, Ma Z, Cheng CH, Berglund AE, Coppola D, et al. Evaluation of invasive breast cancer samples using a 12-chemokine gene expression score: correlation with clinical outcomes. Breast Cancer Res. 2017;19(1):71.
33. Jezequel P, Loussouarn D, Guerin-Charbonnel C, Campion L, Vanier A, Gouraud W, et al. Gene-expression molecular subtyping of triple-negative breast cancer tumours: importance of immune response. Breast Cancer Res. 2015;17:43.
34. Ulloa-Montoya F, Louahed J, Dizier B, Gruselle O, Spiessens B, Lehmann FF, et al. Predictive gene signature in MAGE-A3 antigen-specific cancer immunotherapy. J Clin Oncol. 2013;31(19):2388-95.
35. Hugo W, Zaretsky JM, Sun L, Song C, Moreno BH, Hu-Lieskovan S, et al. Genomic and Transcriptomic Features of Response to Anti-PD-1 Therapy in Metastatic Melanoma. Cell. 2016;165(1):35-44.
36. Goldman MJ, Craft B, Hastie M, Repecka K, McDade F, Kamath A, et al. Visualizing and interpreting cancer genomics data via the Xena platform. Nat Biotechnol. 2020;38(6):675-8.
37. Zhang SS, Chen X, Chen TT, Zhu JW, et al. GSA-Human: Genome Sequence Archive for Human. Yi Chuan. 2021; 43(10):988-993.
38. Li YY, Chung GT, Lui VW, To KF, Ma BB, Chow C, et al. Exome and genome sequencing of nasopharynx cancer identifies NF-kappaB pathway activating mutations. Nat Commun. 2017;8:14121.
39. Bindea G, Mlecnik B, Tosolini M, Kirilovsky A, Waldner M, Obenauf AC, et al. Spatiotemporal dynamics of intratumoral immune cells reveal the immune landscape in human cancer. Immunity. 2013;39(4):782-95.

40. Charoentong P, Finotello F, Angelova M, Mayer C, Efremova M, Rieder D, et al. Pan-cancer Immunogenomic Analyses Reveal Genotype-Immunophenotype Relationships and Predictors of Response to Checkpoint Blockade. Cell Rep. 2017;18(1):248-62.
41. Newman AM, Liu CL, Green MR, Gentles AJ, Feng W, Xu Y, et al. Robust enumeration of cell subsets from tissue expression profiles. Nat Methods. 2015;12(5):453-7.
42. Yoshihara K, Shahmoradgoli M, Martinez E, Vegesna R, Kim H, Torres-Garcia W, et al. Inferring tumour purity and stromal and immune cell admixture from expression data. Nat Commun. 2013;4:2612.
43. Hanzelmann S, Castelo R, Guinney J. GSVA: gene set variation analysis for microarray and RNA-seq data. BMC Bioinformatics. 2013;14:7.
44. Mootha VK, Lindgren CM, Eriksson KF, Subramanian A, Sihag S, Lehar J, et al. PGC-1alpha-responsive genes involved in oxidative phosphorylation are coordinately downregulated in human diabetes. Nat Genet. 2003;34(3):267-73.
45. Dennis G, Jr., Sherman BT, Hosack DA, Yang J, Gao W, Lane HC, et al. DAVID: Database for Annotation, Visualization, and Integrated Discovery. Genome Biol. 2003;4(5):P3.
46. Wilkerson MD, Hayes DN. ConsensusClusterPlus: a class discovery tool with confidence assessments and item tracking. Bioinformatics. 2010;26(12):1572-3.
47. Liu Z, Zhao Q, Zuo ZX, Yuan SQ, Yu K, Zhang Q, et al. Systematic Analysis of the Aberrances and Functional Implications of Ferroptosis in Cancer. iScience. 2020;23(7):101302.
48. Malta TM, Sokolov A, Gentles AJ, Burzykowski T, Poisson L, Weinstein JN, et al. Machine Learning Identifies Stemness Features Associated with Oncogenic Dedifferentiation. Cell. 2018;173(2):338-54 e15.
49. Geeleher P, Cox NJ, Huang RS. Clinical drug response can be predicted using baseline gene expression levels and in vitro drug sensitivity in cell lines. Genome Biol. 2014;15(3):R47.
50. Jiang P, Gu S, Pan D, Fu J, Sahu A, Hu X, et al. Signatures of T cell dysfunction and exclusion predict cancer immunotherapy response. Nat Med. 2018;24(10):1550-8.
51. Simon N, Friedman J, Hastie T, Tibshirani R. Regularization Paths for Cox's Proportional Hazards Model via Coordinate Descent. J Stat Softw. 2011;39(5):1-13.
52. Sveen A, Ågesen TH, Nesbakken A, et al. ColoGuidePro: a prognostic 7-gene expression signature for stage III colorectal cancer patients. Clin Cancer Res. 2012;18(21):6001-10.
53. Bagaev A, Kotlov N, Nomie K, Svekolkin V, Gafurov A, Isaeva O, et al. Conserved pan-cancer microenvironment subtypes predict response to immunotherapy. Cancer Cell. 2021;39(6):845-65 e7.
54. Cao R, Yuan L, Ma B, Wang G, Tian Y. Tumour microenvironment (TME) characterization identified prognosis and immunotherapy response in muscle-invasive bladder cancer (MIBC). Cancer Immunol Immunother. 2021;70(1):1-18.
55. Bader JE, Voss K, Rathmell JC. Targeting Metabolism to Improve the Tumor Microenvironment for Cancer Immunotherapy. Mol Cell. 2020;78(6):1019-33.

56. Adams S, Loi S, Toppmeyer D, Cescon DW, De Laurentiis M, Nanda R, et al. Pembrolizumab monotherapy for previously untreated, PD-L1-positive, metastatic triple-negative breast cancer: cohort B of the phase II KEYNOTE-086 study. Ann Oncol. 2019;30(3):405-11.
57. Adams S, Schmid P, Rugo HS, Winer EP, Loirat D, Awada A, et al. Pembrolizumab monotherapy for previously treated metastatic triple-negative breast cancer: cohort A of the phase II KEYNOTE-086 study. Ann Oncol. 2019;30(3):397-404.
58. Qin Y, Deng J, Zhang L, Yuan J, Yang H, Li Q. Tumor microenvironment characterization in triple-negative breast cancer identifies prognostic gene signature. Aging (Albany NY). 2021;13(4):5485-505.
59. Yi J, Zhong W, Wu H, Feng J, Zouxu X, Huang X, et al. Identification of Key Genes Affecting the Tumor Microenvironment and Prognosis of Triple-Negative Breast Cancer. Front Oncol. 2021;11:746058.
60. Yang A, Wu M, Ni M, Zhang L, Li M, Wei P, et al. A risk scoring system based on tumor microenvironment cells to predict prognosis and immune activity in triple-negative breast cancer. Breast Cancer. 2022.
61. Chen DS, Mellman I. Elements of cancer immunity and the cancer-immune set point. Nature. 2017;541(7637):321-30.
62. Turley SJ, Cremasco V, Astarita JL. Immunological hallmarks of stromal cells in the tumour microenvironment. Nat Rev Immunol. 2015;15(11):669-82.
63. Gajewski TF, Woo SR, Zha Y, Spaapen R, Zheng Y, Corrales L, et al. Cancer immunotherapy strategies based on overcoming barriers within the tumor microenvironment. Curr Opin Immunol. 2013;25(2):268-76.
64. Kim JM, Chen DS. Immune escape to PD-L1/PD-1 blockade: seven steps to success (or failure). Ann Oncol. 2016;27(8):1492-504.
65. Schmid P, Rugo HS, Adams S, Schneeweiss A, Barrios CH, Iwata H, et al. Atezolizumab plus nab-paclitaxel as first-line treatment for unresectable, locally advanced or metastatic triple-negative breast cancer (IMpassion130): updated efficacy results from a randomised, double-blind, placebo-controlled, phase 3 trial. Lancet Oncol. 2020;21(1):44-59.
66. Emens LA, Adams S, Barrios CH, Dieras V, Iwata H, Loi S, et al. First-line atezolizumab plus nab-paclitaxel for unresectable, locally advanced, or metastatic triple-negative breast cancer: IMpassion130 final overall survival analysis. Ann Oncol. 2021;32(8):983-93.
67. Mao X, Xu J, Wang W, Liang C, Hua J, Liu J, et al. Crosstalk between cancer-associated fibroblasts and immune cells in the tumor microenvironment: new findings and future perspectives. Mol Cancer. 2021;20(1):131.
68. Boutilier AJ, Elsawa SF. Macrophage Polarization States in the Tumor Microenvironment. Int J Mol Sci. 2021;22(13).
69. Kwak T, Wang F, Deng H, Condamine T, Kumar V, Perego M, et al. Distinct Populations of Immune-Suppressive Macrophages Differentiate from Monocytic Myeloid-Derived Suppressor Cells in Cancer. Cell Rep. 2020;33(13):108571.

70. Yang L, Shi P, Zhao G, Xu J, Peng W, Zhang J, et al. Targeting cancer stem cell pathways for cancer therapy. Signal Transduct Target Ther. 2020;5(1):8.
71. Clara JA, Monge C, Yang Y, Takebe N. Targeting signalling pathways and the immune microenvironment of cancer stem cells - a clinical update. Nat Rev Clin Oncol. 2020;17(4):204-32.
72. Ruiu R, Tarone L, Rolih V, Barutello G, Bolli E, Riccardo F, et al. Cancer stem cell immunology and immunotherapy: Harnessing the immune system against cancer's source. Prog Mol Biol Transl Sci. 2019;164:119-88.
73. Cazet AS, Hui MN, Elsworth BL, Wu SZ, Roden D, Chan CL, et al. Targeting stromal remodeling and cancer stem cell plasticity overcomes chemoresistance in triple negative breast cancer. Nat Commun. 2018;9(1):2897.
74. O'Conor CJ, Chen T, Gonzalez I, Cao D, Peng Y. Cancer stem cells in triple-negative breast cancer: a potential target and prognostic marker. Biomark Med. 2018;12(7):813-20.
75. Ooko E, Saeed ME, Kadioglu O, Sarvi S, Colak M, Elmasaoudi K, et al. Artemisinin derivatives induce iron-dependent cell death (ferroptosis) in tumor cells. Phytomedicine. 2015;22(11):1045-54.
76. Yamaguchi H, Hsu JL, Chen CT, Wang YN, Hsu MC, Chang SS, et al. Caspase-independent cell death is involved in the negative effect of EGF receptor inhibitors on cisplatin in non-small cell lung cancer cells. Clin Cancer Res. 2013;19(4):845-54.
77. Dent R, Trudeau M, Pritchard KI, Hanna WM, Kahn HK, Sawka CA, et al. Triple-negative breast cancer: clinical features and patterns of recurrence. Clin Cancer Res. 2007;13(15 Pt 1):4429-34.
78. Bauer KR, Brown M, Cress RD, Parise CA, Caggiano V. Descriptive analysis of estrogen receptor (ER)-negative, progesterone receptor (PR)-negative, and HER2-negative invasive breast cancer, the so-called triple-negative phenotype: a population-based study from the California cancer Registry. Cancer. 2007;109(9):1721-8.
79. Wculek SK, Cueto FJ, Mujal AM, Melero I, Krummel MF, Sancho D. Dendritic cells in cancer immunology and immunotherapy. Nat Rev Immunol. 2020;20(1):7-24.
80. Sabado RL, Balan S, Bhardwaj N. Dendritic cell-based immunotherapy. Cell Res. 2017;27(1):74-95.
81. Wang SS, Liu W, Ly D, Xu H, Qu L, Zhang L. Tumor-infiltrating B cells: their role and application in anti-tumor immunity in lung cancer. Cell Mol Immunol. 2019;16(1):6-18.
82. Guzman-Genuino RM, Hayball JD, Diener KR. Regulatory B Cells: Dark Horse in Pregnancy Immunotherapy? J Mol Biol. 2021;433(1):166596.
83. Raskov H, Orhan A, Christensen JP, Gögenur I. Cytotoxic CD8+ T cells in cancer and cancer immunotherapy. Br J Cancer. 2021;124(2):359-367.
84. O'Donnell JS, Teng MWL, Smyth MJ. Cancer immunoediting and resistance to T cell-based immunotherapy. Nat Rev Clin Oncol. 2019;16(3):151-167.
85. Zhang Q, Cheng L, Qin Y, et al. SLAMF8 expression predicts the efficacy of anti-PD1 immunotherapy in gastrointestinal cancers. Clin Transl Immunology. 2021;10(10):e1347.

86. Kalaora S, Lee JS, Barnea E, Levy R, et al. Immunoproteasome expression is associated with better prognosis and response to checkpoint therapies in melanoma. Nat Commun. 2020;11(1):896.
87. Zou Y, Liu B, Li L, Yin Q, Tang J, Jing Z, Huang X, Zhu X, Chi T. IKZF3 deficiency potentiates chimeric antigen receptor T cells targeting solid tumors. Cancer Lett. 2022;524:121-130.
88. Fujiwara Y, Torphy RJ, Sun Y, Miller EN, Ho F, Borcherding N, Wu T, Torres RM, Zhang W, Schulick RD, Zhu Y. The GPR171 pathway suppresses T cell activation and limits antitumor immunity. Nat Commun. 2021;12(1):5857.

Figures

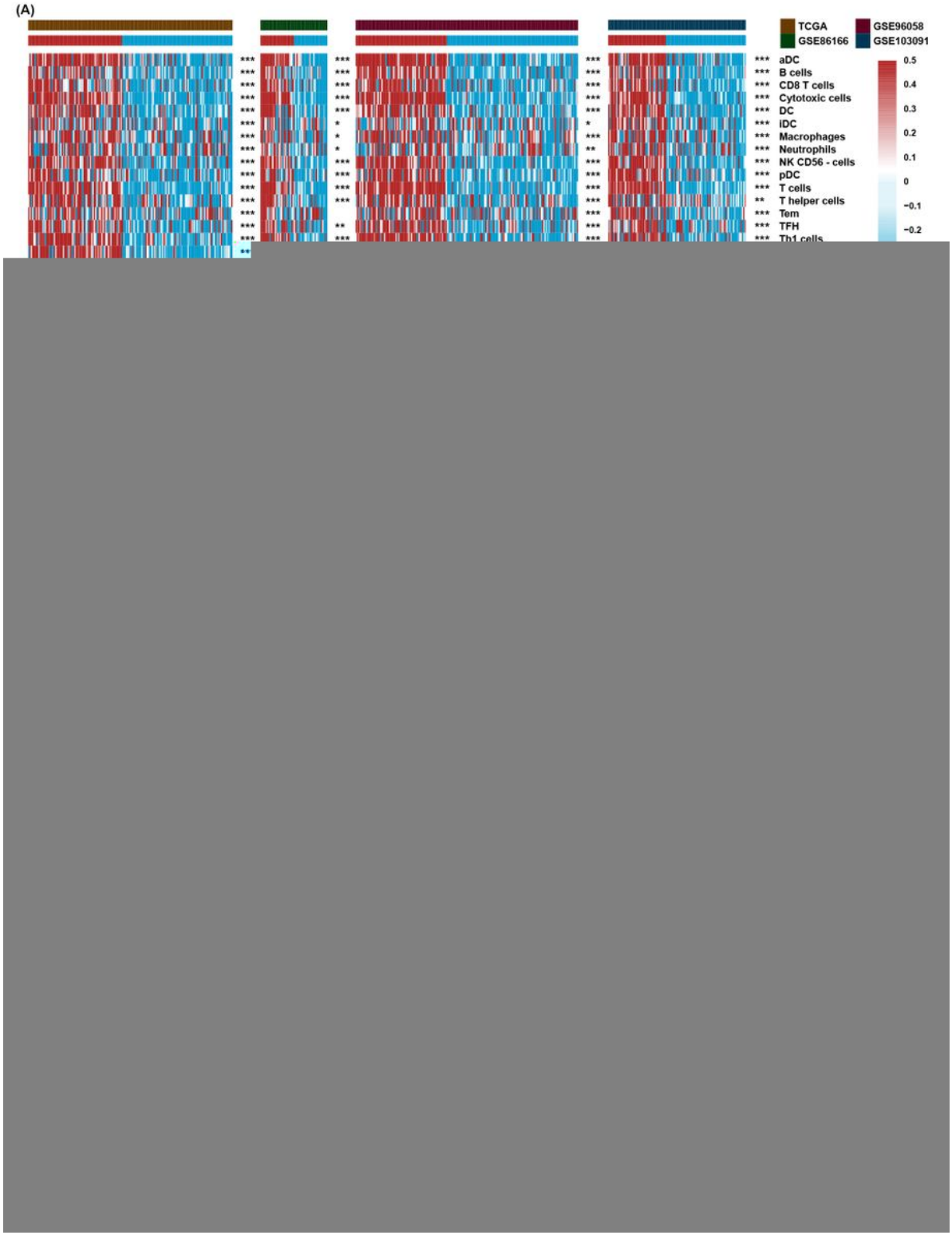

Figure 1

Identification of TME Subtypes. (A) Clustering heatmap of immune cell infiltration levels calculated with immune cell signature 1 in four TNBC cohorts. (B) Immune cell infiltration levels were calculated with immune cell signature 2 in the TNBC cohort between the two TME subtypes. (C) The CIBERSORT algorithm assessed the relative percentage of different immune cell types in a single sample in the whole TNBC cohort. (D) Differences in immune cell type relative percentages assessed by the CIBERSORT

algorithm in a single sample in the whole TNBC cohort. (E) Survival analysis for TME subtypes in the whole TNBC cohort. The asterisks represent the statistical p value (*P < 0.05; **P < 0.01; ***P < 0.001).

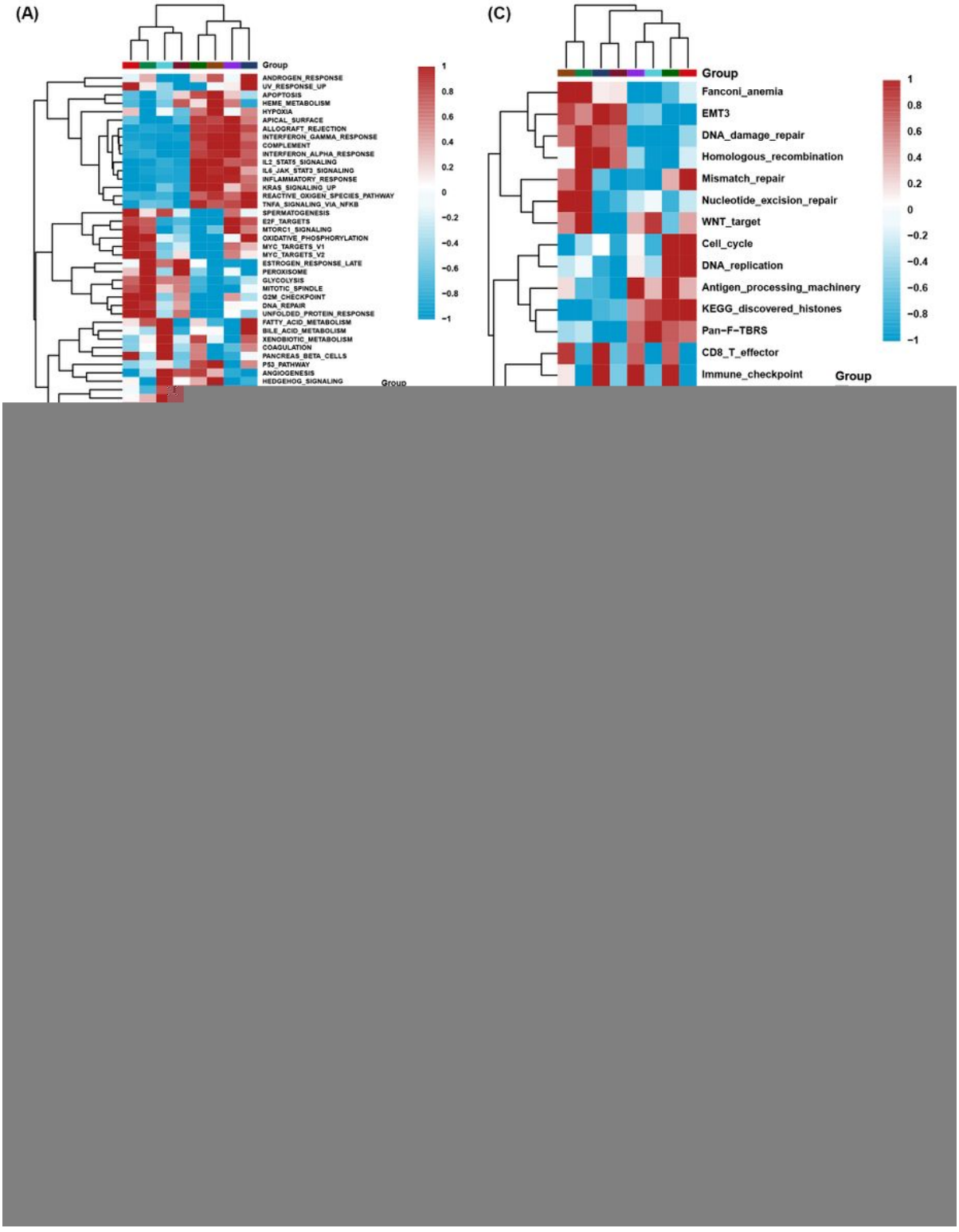

Figure 2

Biological function analysis between TME subtypes. (A) Heatmap of the GSVA enrichment score in curated pathways in four TNBC cohorts. (B) Differences in GSVA enrichment scores in curated pathways in the whole TNBC cohort. (C) Heatmap of curated pathways calculated with another pathway signature in four TNBC cohorts. (D) Differences in curated pathways were calculated with another pathway signature in the whole TNBC cohort. (E) Differentially expressed peaks were identified between the two TME subtypes in TCGA. (F) GO analysis of differentially expressed peaks between two TME subtypes in TCGA. The asterisks represent the statistical p value (*P < 0.05; **P < 0.01; ***P < 0.001).

Figure 4

The role of the TME score in therapeutic efficacy. (A) Correlation analysis between TME score and prediction IC50 values in the whole TNBC cohort. The green line represents that the predicted IC50 of drugs was positively correlated with the TME score, and the red line represents a negative correlation. (B) The difference in TME scores between immunotherapy respondents and nonresponders in TIDE analysis in the whole TNBC cohort. (C) Correlation analysis between the TME score and the results of TIDE analysis in four TNBC cohorts. (D) The correlation analysis between the TME score and the immune cell infiltration levels was calculated with immune cell signature 1 in TCGA pancancer. (E) Survival analyses for patients treated with anti-PD-L1 immunotherapy stratified by both TME score and TMB. (F) Correlation analysis between the TME score and immune cell infiltration levels calculated by immune cell signatures 1 and 2 in the IMvigor210 trial. (G) Differences in TME scores between the CR/PR/SD group and the PD group in the IMvigor210 trial. (H) Rating clinical response to anti-PD-L1 immunotherapy in high or low TME score groups in the IMvigor210 cohort using the chi-square test. (I) Differences in TME scores among immune phenotypes in the IMvigor210 trial. (J) Correlation analysis between the TME score and the immune cell infiltration levels calculated with immune cell signature 1 in GSE35640. (K) The difference in TME scores between immunotherapy respondents and nonresponders in GSE35640. (L) Correlation analysis between the TME score and the immune cell infiltration levels calculated with immune cell signature 1 in GSE78220. The asterisks represent the statistical p value (*P < 0.05; ***P < 0.001).

Supplementary Files

This is a list of supplementary files associated with this preprint. Click to download.

- additionalfile2.xlsx
- S1.jpg

- S2.jpg
- S3.jpg
- S5.jpg
- S6.jpg